molecular pharmaceutics

Article

Cite This: Mol. Pharmaceutics 2019, 16, 2394−2404

pubs.acs.org/molecularpharmaceutics

A Colloid Approach to Self-Assembling Antibodies

Nicholas Skar-Gislinge,[†,‡,∥] Michela Ronti,[¶,⊥] Tommy Garting,[†] Christian Rischel,[‡] Peter Schurtenberger,[†,#] Emanuela Zaccarelli,[*,§] and Anna Stradner[*,†,#]

[†]Physical Chemistry, Department of Chemistry, Lund University, SE-221 00 Lund, Sweden

[‡]Novo Nordisk A/S, DK-2760 Malov, Denmark

[¶]Department of Physics, Sapienza Università di Roma, Piazzale Aldo Moro 2, 00185 Rome, Italy

[§]Institute for Complex Systems, National Research Council (ISC-CNR), Uos Sapienza and Department of Physics, Sapienza Università di Roma, Piazzale Aldo Moro 5, 00185 Rome, Italy

[#]LINXS - Lund Institute of Advanced Neutron and X-ray Science, Scheelevägen 19, SE-223 70 Lund, Sweden

Supporting Information

ABSTRACT: Concentrated solutions of monoclonal antibodies have attracted considerable attention due to their importance in pharmaceutical formulations; yet, their tendency to aggregate and the resulting high viscosity pose considerable problems. Here we tackle this problem by a soft condensed matter physics approach, which combines a variety of experimental measurements with a patchy colloid model, amenable of analytical solution. We thus report results of structural antibodies and dynamic properties obtained through scattering methods and microrheological experiments. We model the data using a colloid-inspired approach, explicitly taking into account both the anisotropic shape of the molecule and its charge distribution. Our simple patchy model is able to disentangle self-assembly and intermolecular interactions and to quantitatively describe the concentration-dependence of the osmotic compressibility, collective diffusion coefficient, and zero shear viscosity. Our results offer new insights on the key problem of antibody formulations, providing a theoretical and experimental framework for a quantitative assessment of the effects of additional excipients or chemical modifications and a prediction of the resulting viscosity.

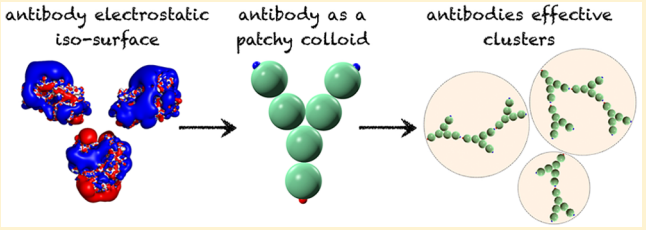

KEYWORDS: *antibodies, self-assembly, patchy colloids*

INTRODUCTION

Immunoglobulin gamma (IgG) constitutes the major antibody isotype found in serum and takes part in the immune response following an infection to the body. IgGs contain three structured domains: two antigen binding domains (FAB) and one so-called constant domain (FC) arranged in a Y-shape via a flexible hinge region. The specific details of the hinge region and the FC further classify the IgGs into four subclasses: IgG1, IgG2, IgG3, and IgG4. In the biopharmaceutical industry, monoclonal antibodies (mAb) based on IgGs are a major platform for potential drug candidates, with more than 20 mAb-based drugs available on the market and more in development.[1,2] The popularity of these macromolecules is due to a large flexibility in molecular recognition thanks to the variable portions of the FAB, a long half-life time in the body, and the possibility of humanization minimizing the risk of immunogenicity.

In order for mAbs to become a successful pharmaceutical product, not only a biological effect but also a high chemical and formulation stability of the solutions is required. Generally, for mAb-based drugs, a high concentration formulation of the order of 100 g/L or more is desirable.[3,4] However, in many cases, mAb solutions at these concentrations exhibit dramatically altered flow properties, resulting in serious challenges during production and when administering the drug.

The flow properties of protein solutions are primarily determined by the shape of the proteins and their mutual interactions. As the concentration increases, protein−protein interactions become increasingly significant. Despite the extensive experimental and theoretical work devoted to protein crowding and its effects on the resulting stability and flow properties at high protein concentration, our ability to predict for example the concentration-dependence of the zero shear viscosity η_0 and the location of an arrest or glass transition is still limited.[5−12] For antibody solutions, this is a particularly difficult problem as attractive interactions often lead to reversible self-association between the antibody molecules,[7,9] making the change in solution flow properties highly sensitive to the protein concentration.[13,14]

A number of studies have made attempts to characterize cluster formation in mAb solutions and to interpret antibody

Received: January 7, 2019
Revised: May 1, 2019
Accepted: May 6, 2019
Published: May 6, 2019

DOI: 10.1021/acs.molpharmaceut.9b00019
Mol. Pharmaceutics 2019, 16, 2394−2404

solution properties through analogies with colloids or polymers. In particular, scattering techniques were used to investigate protein interactions and self-association in antibody formulations.[7,9,15−18] While investigations of the self-association behavior of various mAb formulations have frequently addressed mAb self-association and its effect on flow properties, we are far from having any predictive understanding and a generally accepted methodology and/or theoretical framework to detect antibody association and model mAb interactions quantitatively. A particular difficulty here is that while the nonspherical shape and internal flexibility has sometimes been addressed, interactions between proteins are frequently treated based on spherical approximations, and in particular, the enormous effect that specific, directional interactions can have is generally not considered.

Here we present an investigation of the solution behavior of a monoclonal antibody varying the concentration, where we combine scattering methods and viscosity measurements with theoretical calculations and Monte Carlo (MC) simulations. We explicitly consider in our model the anisotropy of both the shape and the interactions of the antibody molecules. To this aim, we focus on Y-shaped molecules interacting within a simple patchy model that is built from calculations of the electrostatic properties of the considered mAbs. The simplicity of the model allows for analytical treatment through Wertheim theory,[19] yielding all thermodynamic properties of the solution and in particular the compressibility that can be directly compared to the experimentally determined osmotic compressibility or apparent molecular weight. In addition, we calculate the size distribution of mAb clusters using the hyperbranched polymer theory (HPT),[20] without introducing any additional free parameters. Finally, we use MC simulations to verify the results predicted theoretically.

With the explicit cluster size distribution obtained by HPT at all concentrations investigated and assuming that the dynamic solution properties (such as the apparent hydrodynamic radius $R_{h,app}$ or the relative viscosity $\eta_r = \eta_0/\eta_s$, where η_0 is the zero shear viscosity of the antibody solution, and η_s is the solvent viscosity) are primarily determined by excluded volume effects, we are able to make an additional coarse-graining step, in which we model the mAb clusters as effective hard (HS) or sticky (or adhesive) hard (SHS) spheres, for which quantitative relationships for the concentration-dependence of $R_{h,app}$ and η_r exist. We find that the measured data are indeed well reproduced by this model, confirming that excluded volume interactions between the assembled clusters are at the origin of the strong increase of η_r with increasing concentration. Hence, our simple model is capable of quantitatively predicting the measured concentration-dependence of the viscosity, solely based on static and dynamic light scattering experiments. Our results can be easily generalized to different types of mAbs, salt concentrations and temperature and may provide a crucial step for a proper description of self-association and dynamics of monoclonal antibodies.

EXPERIMENTAL SECTION

Sample Preparation. The mAb used in this study was a humanized IgG4 against trinitrophenyl, which was previously found to exhibit an increased viscosity at high concentrations[5] (where it was labeled mab-C). It was manufactured by Novo Nordisk A/S and purified using Protein A chromatography and subsequently concentrated to 100 mg/mL and buffer exchanged into a 10 mM histidine buffer with 10 mM NaCl at pH 6.5.

For measurements, the sample was diluted and buffer exchanged to a 20 mM histidine pH 6.5 buffer containing 10 mM NaCl and subsequently concentrated using a 100 kD cutoff spin filter (Amicon Inc.). The concentrated sample was used as a stock solution for preparing the less concentrated solutions. The concentration of each sample was determined by a series of dilutions followed by measurement of the absorption at 280 nm using an extinction coefficient of $\epsilon^{280nm}_{1\%,1cm} = 1.489$. In order to assess the uncertainty of the concentration determination, the dilution series was done in triplicates.

Light Scattering. The dynamic (DLS) and static (SLS) light scattering experiments were made using a 3D-LS Spectrometer (LS Instruments AG, Switzerland) with a 632 nm laser, recording DLS and SLS data simultaneously. The measurements were conducted at a 90° scattering angle. Before measurement, the samples were transferred to precleaned 5 mm NMR tubes and centrifuged at 3000*g* and 25 °C for 15 min, to remove any large particles and to equilibrate temperature. Directly after centrifugation, the samples were placed in the temperature equilibrated sample vat, and the measurement was started after 5 min to allow for thermal equilibration. Additional low concentration SLS measurements were done using a HELIOS DAWN multiangle light scattering instrument (Wyatt Technology Corporation, CA, USA), connected to a concentration gradient pump. The instruments were calibrated to absolute scale using toluene (with a Rayleigh ratio of $1.37\cdot10^{-5}$ cm^{-1} at 25 °C and $\lambda = 632.8$ nm), in the case of the 3D-LS Spectrometer, and toluene and a secondary protein standard with a known molecular mass for the HELIOS DAWN, allowing for direct comparison of the two data sets.

From the static light scattering experiments, the apparent weight average molecular weight $\langle M\rangle_{w,app}$ of the antibodies in solution was calculated using

$$\langle M\rangle_{w,app} = \frac{R(90)}{KC} \tag{1}$$

where $R(90)$ is the absolute excess scattering intensity or excess Rayleigh ratio measured at a scattering angle of 90°, $K = 4\pi^2 n^2 (dn/dC)^2/N_A\lambda_0^4$, n is the refractive index of the solution, $dn/dC = 0.192$ mL/*g* is the refractive index increment of the antibodies, λ_0 is the vacuum wavelength of the laser, and C is the antibody concentration in mg/mL. The excess Rayleigh ratio $R(90)$ is obtained from the measured scattering of the protein solution, $I(90)$, the solvent $I_s(90)$, and the reference standard $I_{ref}(90)$ using $R(90) = [(I(90) - I_s(90))/I_{ref}(90)]R_{ref}(n/n_{ref})^2$, where R_{ref} is the Rayleigh ratio of the reference solvent, and n and n_{ref} are the index of refraction of the solution and the reference solvent, respectively. Note that, because of the small size of the antibody molecules and of the antibody clusters, there is no measurable angular-dependence in the scattering intensity, and we can directly use the intensity values measured at a scattering angle of 90° instead of the corresponding values extrapolated to $\theta = 0$.

In the DLS experiments, the apparent *z*-average diffusion coefficient $\langle D\rangle_{z,app}$ of the antibodies was extracted from the measured intensity autocorrelation function $g_2(\tau)$, where τ is the delay time. Using a first order cumulant analysis of the initial 20% of the decay of $g_2(\tau)$ (except for the highest concentrations where a second order cumulant analysis was necessary), the apparent hydrodynamic radius $\langle R_h\rangle_{z,app}$ was

DOI: 10.1021/acs.molpharmaceut.9b00019
Mol. Pharmaceutics 2019, 16, 2394−2404

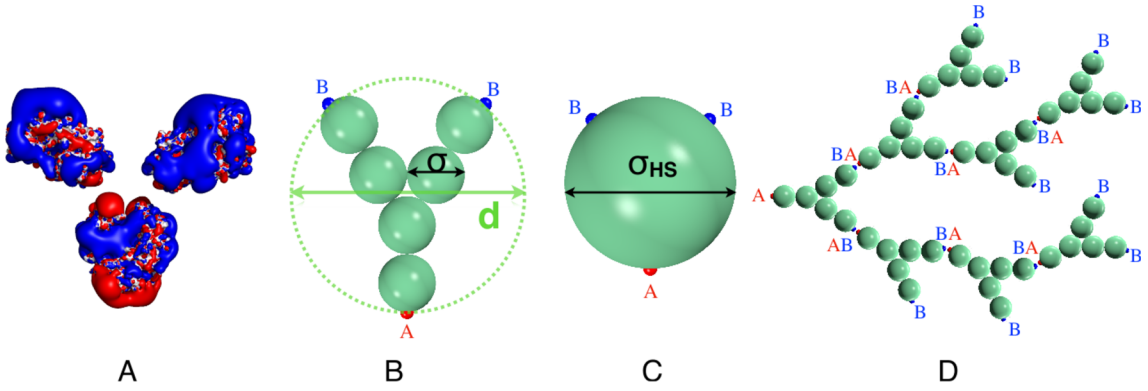

Figure 1. Design of the patchy model of mAbs. (a) Isosurfaces of the −1 (red) and +1 k_BT (blue) electrostatic potential at pH 6.5 with 10 mM NaCl, indicating an overall positive charge for the arms (FAB domains) and a largely negative charge for the tail (FC domain). (b) Illustration of the patchy YAB model: six hard spheres (in green) each of diameter σ are constrained to a rigid Y-shape, constituting a single mAb molecule of geometric diameter d. Each molecule is decorated with one A patch on the tail (red) and two B (blue) patches, one on each arm, mimicking the negative and positive charges respectively. Only AB attractive interactions are considered mimicking the arm-to-tail electrostatic interactions. (c) Representation of the YAB model as an effective patchy hard sphere of diameter σ_{HS} as done in the Wertheim theory; (d) schematic view of the clustering process for mAb molecules forming hyperbranched structures.

calculated using the Stokes−Einstein equation $\langle R_h \rangle_{z,app} = k_BT/(6\pi\eta_s\langle D \rangle_{z,app})$, where k_B is the Boltzmann constant, T is the absolute temperature, and η_s is the solvent viscosity.

Microrheology. The zero shear viscosity η_0 of the antibody solutions relative to that of the pure buffer, denoted as the relative viscosity $\eta_r = \eta_0/\eta_s$, was obtained using DLS-based tracer microrheology. Sterically stabilized (pegylated) latex particles were mixed with protein samples to a concentration of 0.01%v/v using vortexing and transferred to 5 mm NMR tubes. The sterically stabilized particles were prepared by cross-linking 0.75 kDa amine−PEG (polyethylene glycol) (Rapp Polymere, 12750-2) to carboxylate stabilized polystyrene (PS) particles (Thermo Fisher Scientific, C37483) with a diameter of 1.0 μm using EDC (*N*-(3-dimethylaminopropyl)-*N*′-ethyl-carbodiimide) (Sigma Aldrich, 39391) as described in detail in ref 21. DLS measurements were performed on a 3D-LS Spectrometer (LS Instruments AG, Switzerland) at a scattering angle of 46−50° to stay away from the particle form factor minima and thus to maximize the scattering contribution from the tracer particles with respect to the protein scattering. Measurements were made using modulated 3D cross correlation DLS[22] to suppress all contributions from multiple scattering that occur in the attempt to achieve conditions where the total scattering intensity is dominated by the contribution from the tracer particles. Samples were either prepared individually or diluted from more concentrated samples using a particle dispersion with the same particle concentration as in the sample as the diluent. The diffusion coefficient D of the particles was then extracted from the intensity autocorrelation function using a first order cumulant analysis of the relevant decay. This diffusion coefficient is compared to that of tracer particles in a protein-free solvent (buffer) resulting in a relative diffusion coefficient, $D_r = D_{Sample}/D_{Solvent}$. The relative viscosity η_r is related to D_r as $\eta_r = 1/D_r$, again according to the Stokes−Einstein equation, where now R_h is the known and constant hydrodynamic radius of the tracer particles.[21,23]

Theory. We model mAbs as patchy colloids and use a theoretical approach that has been successfully applied to such particles, in order to calculate their structural properties as a function of concentration. Patchy models are coarse-grained descriptions, which condense complex anisotropic interactions, often of electrostatic origin, in simple site−site aggregation, that have been applied in the past to several protein solutions,[24−27] colloidal clays,[28,29] DNA-based nanoconstructs,[30] and other complex systems.[31]

In order to build a meaningful model, it is crucial to identify the key ingredients controlling the intermolecular interactions. A previous study of this antibody has shown that the viscosity is sensitive to the salt concentration, pointing toward electrostatic interactions as a main component of the intermolecular interactions.[5] Therefore, we first carry out a study of the electrostatic isosurface of a single antibody molecule in the considered buffer solution, in order to locate the active spots on the molecule surface that are involved in particle−particle aggregation.

The FAB domains are built using the antibody modeler tool in the Molecular Operating Environment (Chemical Computing Group Inc., Canada) computer program, whereas the FC domain was taken from a crystallographic structure with a similar FC domain found in the protein data bank (PDBID: 4B53). We next carry out electrostatic calculations in a two-step process, using pdb2pqr[32] and the automated Poisson Boltzmann solver[33] (apbs) pymol plugin. The pdb2pqr server is hosted by the National Biomedical Computation Resource at http://nbcr-222.ucsd.edu/pdb2pqr_2.1.1/ and was used to calculate the protonation state of the FAB and FC domains at pH 6.5 taking the local structure around the titratable residues into account. The prepared structures were then used by the apbs plugin to calculate an electrostatic map of the protein. The apbs was run using the default parameters, with the addition of Na+ and Cl− ions corresponding to a salt concentration of 10 mM.

The resulting charge distribution is illustrated in Figure 1a, which clearly shows that the considered mAbs have an overall positively charged surface on the two arms (FAB domains) and a largely negative charge on the tail (FC domain). This suggests that the main driving mechanism for mAbs aggregation has to be an attractive arm-to-tail interaction.

To take into account this result, the antibody molecule is represented as a symmetric *Y*-shaped particle, constructed from six hard spheres of diameter σ, as illustrated in Figure 1b. Each mAb is decorated by three patches, one of type A on the tail and two of type B on the arms. Only AB interactions are taken

DOI: 10.1021/acs.molpharmaceut.9b00019
Mol. Pharmaceutics 2019, 16, 2394−2404

into account based on the charge distribution on the surface of the mAb molecule in the studied buffer conditions, while *AA* and *BB* interactions are not considered. *AB* interactions are modeled as an attractive square-well (SW) potential of range $\delta = 0.5(\sqrt{5 - 2\sqrt{3}} - 1)\sigma \approx 0.119\sigma$, which guarantees that each patch is engaged at most in one bond.[34] For this model, the geometric diameter d of a single mAb molecule is that of the circle tangent to the external spheres: $d = \frac{9+2\sqrt{3}}{3}\sigma$.

Analytical Solution of the YAB Model. To predict the behavior of our patchy model, which we call the YAB model, we use a thermodynamic perturbation theory, introduced by Wertheim roughly 30 years ago, which describes associating molecules under the hypothesis that each sticky site on a particle cannot bind simultaneously to two or more sites on another particle.[19]

In Wertheim theory,[19,35] the YAB molecule is represented as an effective patchy sphere, illustrated in Figure 1c. The free energy F of a system of N patchy spheres in a volume V, with number density $\rho = N/V$, is calculated as the sum of the free energies of a hard sphere reference term F_{HS} plus a bonding term F_b.

The first term is the Carnahan−Starling (CS) free energy[36] of an equivalent HS system, which has to be determined according to the nature of the molecule. For nonspherical molecules, the HS reference system effective diameter σ_{HS} is not known and needs to take into account correctly the excluded volume of the particles. This is established from the comparison to experiments.

The bonding free energy F_b per particle of the YAB model is

$$\beta\frac{F_b}{N} = 2\ln X_B + \ln X_A - X_B - \frac{X_A}{2} + \frac{3}{2} \tag{2}$$

where $\beta = \frac{1}{k_B T}$, and X_A and X_B are the fractions of the nonbonded patch of each species.[37] For the YAB model they are:

$$X_A = \frac{1}{1 + 2\rho\Delta X_B}; \quad X_B = \frac{1}{1 + \rho\Delta X_A} \tag{3}$$

with $\Delta = v_B[e^{\beta\epsilon_0} - 1]\frac{1 - A\eta - B\eta^2}{(1-\eta)^3}$, $v_B = \pi\delta^4\frac{15\sigma + 4\delta}{30\sigma^2}$, $A = \frac{5}{2}\frac{3 + 8\delta/\sigma + 3(\delta/\sigma)^2}{15 + 4\delta/\sigma}$, $B = \frac{3}{2}\frac{12\delta/\sigma + 5(\delta/\sigma)^2}{15 + 4\delta/\sigma}$, and $\eta = \frac{\pi}{6}\rho\sigma^3$.[34,38]

From eq 3, we can calculate the expressions for the fractions of nonbonded patches in terms of density and temperature, as

$$X_A = \frac{2}{1 + \rho\Delta + \sqrt{\rho^2\Delta^2 + 6\rho\Delta + 1}};$$
$$X_B = \frac{\rho\Delta - 1 + \sqrt{\rho^2\Delta^2 + 6\rho\Delta + 1}}{4\rho\Delta} \tag{4}$$

Instead of using these two variables, it is more convenient to refer to the so-called bond probability p, defined as

$$p \equiv p_B = 1 - X_B = \frac{p_A}{2} = \frac{1 - X_A}{2} \tag{5}$$

In order to compare with experimentally measurable quantities such as the static structure factor $S(0)$, we calculate the isothermal compressibility, defined as

$$\kappa_T = -\frac{1}{V}\left(\frac{\partial V}{\partial P}\right)_T = \frac{1}{V}\left(\frac{\partial^2 V}{\partial^2 F}\right)_T \tag{6}$$

as a function of concentration, where P is the pressure, and V is the volume, by simply differentiating twice the analytic free energy with respect to volume.[39] The quantities κ_T and P are the analogues of the osmotic compressibility and of the osmotic pressure in our theoretical model.

Wertheim theory directly predicts the Helmholtz free energy and the thermodynamic properties of the system, including for example the energy per particle, the specific heat at constant volume, and the isothermal compressibility, from the dependence of the bonding probability p on the temperature T and the number density ρ. However, it does not yield the resulting cluster size distribution that would be needed for a comparison with other experimental quantities. To this purpose, we exploit the fact that the YAB model belongs to the class of hyperbranched polymers.[20] Indeed, the YAB molecule is of the kind AB_{f-1} in HPT language with $f = 3$, as shown in Figure 1(d), for which the bond probability p of Wertheim theory defined above is the fraction of bonded B groups, and $(f-1)p$ is the fraction of bonded A groups. For hyperbranched polymers, there is one nonbonded A group for each cluster; therefore, the average number of monomers per cluster is the reciprocal of the fraction of unreacted A groups. Hence, the only input needed to evaluate the cluster size distribution $n(s)$ is the bond probability p, which we get from Wertheim theory. In the YAB model, calling $p(2p)$ the fraction of $B(A)$ patchy sites, the cluster size distribution in the framework of hyperbranched polymer theory is finally given by

$$n(s) = \frac{(2s)!}{s!(s+1)!}p^{s-1}(1-p)^{s+1} \tag{7}$$

where $n(s)$ is the probability of finding clusters of size s for a system with bond probability p. From the cluster size distributions, we then calculate the weight average, the z-average, and the polydispersity of the clusters for each concentration.

In summary, it is possible to calculate the equilibrium cluster size distribution of the clusters solely from the knowledge of the bonding probability p. As this parameter is directly an outcome of Wertheim theory, the YAB model is amenable to a full analytical treatment, allowing one to obtain simultaneously the thermodynamic and the connectivity properties of the solutions, to be directly compared with the experimental results.

RESULTS

Static and Dynamic Properties. The static and dynamic properties of our antibody solutions have been investigated as a function of mAB concentration using the experimental techniques described in the Experimental Section. The results from these experiments are summarized in Figure 3. The static light scattering (SLS) data in Figure 3a show that the apparent molecular weight $\langle M\rangle_{w,app}$ initially increases with concentration C from the known value of the molecular weight of the mAb monomer (i.e., M_1 = 147 000 g/mol), goes through a maximum at a concentration of around $C \approx 30$ mg/mL, and then strongly decreases at higher concentrations. A similar trend can also be seen for the apparent hydrodynamic radius $\langle R_h\rangle_{z,app}$, reported in Figure 3b, that is obtained by dynamic light scattering (DLS). We find that also $\langle R_h\rangle_{z,app}$ initially

DOI: 10.1021/acs.molpharmaceut.9b00019
Mol. Pharmaceutics 2019, 16, 2394−2404

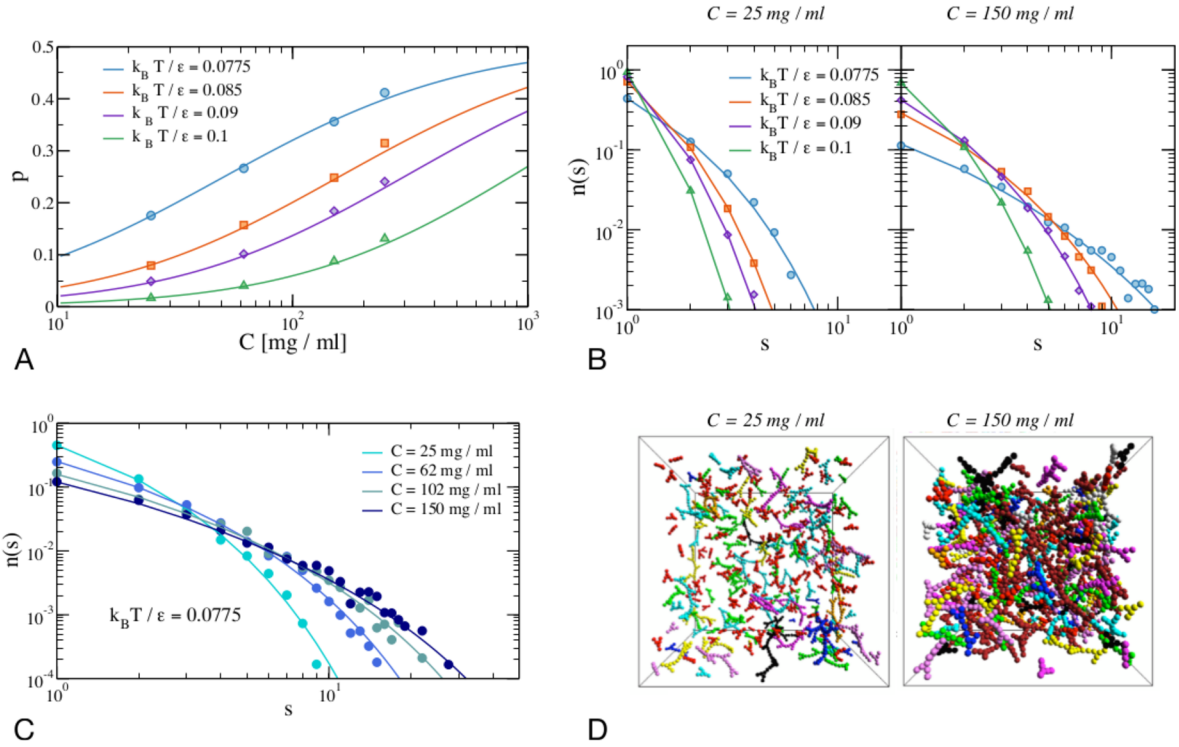

Figure 2. Results from theory (lines) and simulations (symbols). (a) Bond probability p as a function of mAb concentration at different attraction strengths k_BT/ϵ. Small deviations between theory and simulations only occur at high C. (b) Cluster size distributions $n(s)$ for C = 25 mg/mL (left) and C = 150 mg/mL (right) for different k_BT/ϵ. (c) Cluster size distributions $n(s)$ for k_BT/ϵ = 0.0075 and several values of C. (d) Simulation snapshots for C = 25 mg/mL (left) and C = 150 mg/mL (right). Different colors identify different cluster sizes.

increases from the monomer value of $R_{h,1} \approx 6$ nm, reaches a maximum at $C \approx 150$ mg/mL, and finally decreases at higher values of C. In contrast, the reduced viscosity η_r, shown in Figure 3c, monotonically increases with concentration and appears to diverge for $C \approx 200-300$ mg/mL. Qualitatively, the concentration-dependence of the three key quantities $\langle M \rangle_{w,app}$, $\langle R_h \rangle_{z,app}$, and η_r is in agreement with a behavior where the mAbs self-assemble into aggregates with increasing concentration. While this is visible in the SLS and DLS data at low concentrations, the influence of excluded volume effects on the scattering data becomes more prominent at higher concentrations and results in a decrease of the measured values for $\langle M \rangle_{w,app}$ and $\langle R_h \rangle_{z,app}$. At the same time, these increasing interaction effects also result in a corresponding increase of the zero shear viscosity of the mAb solution.

While it is straightforward to qualitatively assess the existence of aggregation and intermolecular interactions, a quantitative interpretation of the experimental data would require knowledge of both the molecular weight distribution of the resulting aggregates as well as the interaction potential between antibodies. This situation is similar to the difficulties encountered when trying to analyze scattering and rheology data of surfactant molecules forming large polymer-like micelles.[40,41] Crucially, a qualitative comparison between the behavior normally encountered for polymer-like micelles and the data shown in Figure 3 shows significant differences. Indeed, for polymer-like micelles, the maxima in $\langle M \rangle_{w,app}$ and $\langle R_h \rangle_{z,app}$ are directly linked to the overlap concentration C^* that marks the transition from a dilute to a semidilute concentration regime and thus occur at approximately the same value. For the mAb data shown in Figure 3, however, there exists a large difference between the concentrations related to the maxima in $\langle M \rangle_{w,app}$ and $\langle R_h \rangle_{z,app}$, respectively. This clearly indicates that a simple application of polymer models, such as the worm-like chain model previously used successfully to, for example, describe SLS and DLS data for antigen−mAb complexes,[42] does not work. We thus instead exploit analogies to patchy colloids in order to design a coarse-grained model for our system and investigate whether we can obtain with this approach a quantitative analysis of the experimental data.

Monte Carlo Simulations of the YAB Model and Comparison to the Analytical Treatment. We complement the theoretical approach with Monte Carlo simulations of the YAB model, shown in Figure 1b, in order to validate the analytical results. We perform standard MC simulations of N = 1000 YAB particles at different number densities $\rho = N/V$, where V is the volume of the cubic simulation box. The unit of length is σ. To compare the experimental value of C with simulations and theory, we consider the geometric radius $d/2$ of the Y-colloid equal to the hydrodynamic radius measured for a single mAb molecule, which is ∼6 nm. With this choice, we have that $\sigma \approx 2.9$ nm, and considering that the mass of a molecule is 150 kDa, an experimental concentration of 1 mg/mL corresponds to $\sim 9.7 \times 10^{-5}/\sigma^3$ in simulation units.

The mAbs modeled as patchy Y-shaped colloids self-associate into clusters with increasing concentration through reversible AB bonds, as a result from the attraction between A and B patches. Their assembly can be monitored by focusing on the variation of the bond probability p and the distribution $n(s)$ of clusters of size s as a function of the two parameters controlling the assembly: the attractive strength k_BT/ϵ, where ϵ is the well depth of the square-well attraction between A and B patches and the mAb concentration C.

DOI: 10.1021/acs.molpharmaceut.9b00019
Mol. Pharmaceutics 2019, 16, 2394−2404

We report in Figure 2 some representative results comparing theory and simulations, including the bond probability and the cluster size distributions for different concentrations and attraction strengths. In all cases, we find that there is quantitative agreement between theory and simulations for both thermodynamic and cluster observables. Thus, we can confidently use the results of the theoretical approach in order to compare with experimental results.

Structural Properties of the Antibody Solutions Described by the YAB Patchy Model. We are now able to report a direct comparison between the analytical results for the YAB patchy model and experiments, particularly for the apparent molecular weight $\langle M \rangle_{w,app}$ shown in Figure 3(a). To

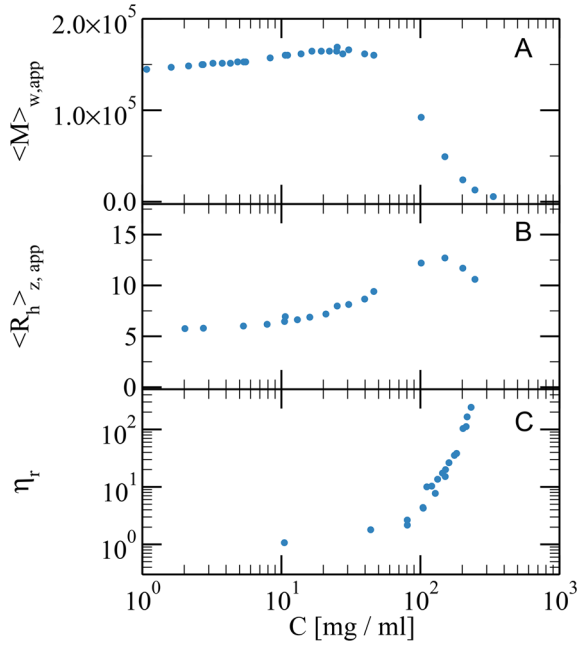

Figure 3. Experimental results for the concentration-dependence of the mAb solutions. (a) Apparent molecular weight $\langle M \rangle_{w,app}$ in units of g/mol vs weight concentration C as determined by static light scattering. (b) Apparent hydrodynamic radius $\langle R_h \rangle_{z,app}$ in units of nm vs weight concentration C from dynamic light scattering. (c) Relative viscosity η_r vs weight concentration C measured by DLS-based microrheology.

this aim, we calculate the isothermal compressibility $\kappa_T = -1/V(\partial V/\partial P)_T$ for our YAB model, since κ_T is related to $S(0)$, the static structure factor at $q = 0$, as

$$S(0) = \rho k_B T \kappa_T \tag{8}$$

$S(0)$ in turn is related to the experimentally determined apparent weight average molar mass by $\langle M \rangle_{w,app} = M_1 S(0)$, where M_1 is the molar mass of a monomer. In a solution where antibodies self-assemble into larger clusters described via Wertheim theory, static light scattering thus provides an apparent weight average cluster size (or apparent weight average aggregation number) $\langle s \rangle_{w,app}$ simply given by

$$\langle s \rangle_{w,app} = \frac{\langle M \rangle_{w,app}}{M_1} = S(0) \tag{9}$$

By normalizing the measured apparent molecular weight by the antibody molecular weight, we can compare $S(0)$ calculated directly from Wertheim theory with the measured apparent average cluster size from static light scattering. However, since mAbs are not spherical as assumed in Wertheim theory, we need to determine the HS reference system. To this aim, we define an equivalent hard sphere diameter σ_{HS} of the Y-molecule, also shown in Figure 1(c), and use it as a free parameter in the theory, together with the energy strength of AB bonds $k_B T/\epsilon$. We thus calculate κ_T for different values of σ_{HS} and $k_B T/\epsilon$ and fit the theoretical results to the experiments as described in the Supporting Information. Figure 4 compares $\langle s \rangle_{w,app}$ for the YAB model with the SLS

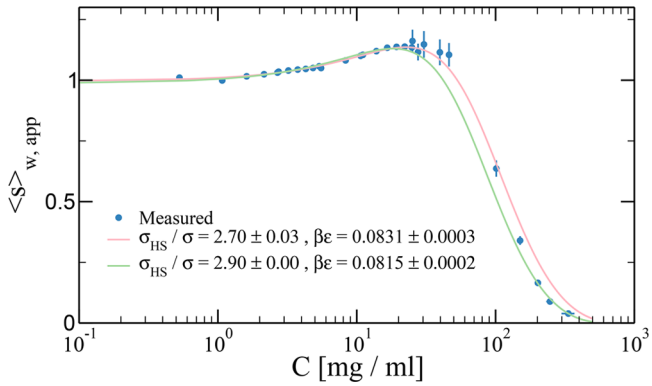

Figure 4. Comparison of SLS data with patchy model predictions. Experimental $\langle s \rangle_{w,app}$ compared with YAB model results: the best agreement, particularly for high concentration data, is obtained for an equivalent hard sphere diameter $\sigma_{HS} = 2.9\sigma \approx 4.2$ nm and $\epsilon/k_B T \approx 12.3$.

data, finding that the best fit is obtained with an effective hard sphere diameter of $\sigma_{HS} = 2.9\sigma$ and a strength of the AB patch–patch attraction given by $\epsilon \simeq 12.3 k_B T$, which also correctly describe the high concentration behavior that is most relevant for the viscosity to be discussed later. Note that the estimated value of σ_{HS} is considerably smaller than the geometric diameter of the YAB molecule (see Figure 1(b)), thus accounting for the penetrability of the Y-shaped antibodies. When converted into real units, an effective HS radius of 4.2 nm is found, which also compares well with the measured radius of gyration of the antibody molecule $R_g \approx 4.7$ nm.

Dynamic Properties Described by a Coarse-Grained Model of Antibody Clusters. Having analyzed the SLS data using Wertheim theory, we now have a prediction for the effect of concentration on the self-assembling behavior of mAbs, and we can thus calculate the cluster size distributions $n(s)$ at all concentrations thanks to HPT. Next, we make an attempt to test the consistency of these results with the data obtained using DLS for the same samples shown in Figure 3b. Unfortunately, this is much less straightforward than the analysis of the SLS data and requires an additional coarse-graining step, illustrated in Figure 5.

The main problem here is that we currently lack a theoretical model that would allow us to calculate the effective or apparent hydrodynamic radius $\langle R_h \rangle_{app}$ of concentrated solutions of polydisperse antibody clusters. We thus propose an approach in which we use the self-assembled clusters of the patchy model and treat them as new interacting objects. Their dominant interaction is of course excluded volume, and hence, we consider them as effective polydisperse hard spheres, each with its own radius resulting from its size s in terms of monomers. To go one more step, we also consider them as sticky hard spheres.

DOI: 10.1021/acs.molpharmaceut.9b00019
Mol. Pharmaceutics 2019, 16, 2394–2404

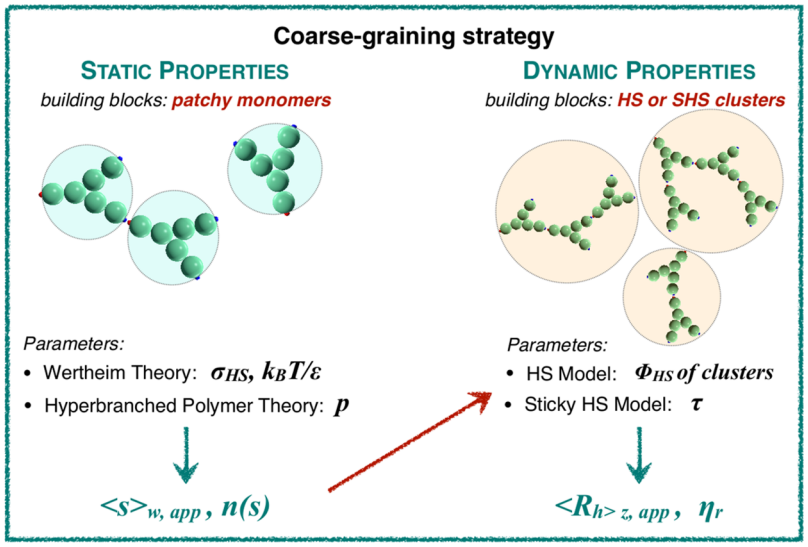

Figure 5. Coarse-graining strategy used to analyze the concentration-dependent cluster formation and its effects on the structural and dynamic properties of the solution.

Within this approach, we first calculate the *z*-average[43] hydrodynamic radius $\langle R_h \rangle_z$ of the mAb solutions using the cluster size distributions obtained theoretically. Next, we model the solutions at each concentration as dispersions of colloids with a size given by $\langle R_h \rangle$ and an effective hard sphere volume fraction ϕ_{HS}. The influence of interparticle interactions on the resulting collective diffusion coefficient, or $\langle R_h \rangle_{z,app}$, is calculated by treating the spheres either as hard or sticky hard spheres, for which accurate expressions exist.

First, we need to determine the conformationally averaged hydrodynamic radius $\langle R_h(s) \rangle$ of mAb clusters with a given size *s*. For each value of *s*, clusters of mAbs were generated randomly, where the clusters also have to satisfy the criterion of self-avoidance and where each monomer in a cluster is allowed to have a maximum of three connections (i.e., reflecting the YAB structure imposed by our model, more details are provided in the Supporting Information). For each individual cluster conformation, its hydrodynamic radius $R_h(s)$ is then calculated using the program Hydropro,[44] and conformationally averaged values $\langle R_h(s) \rangle$ are calculated from 100 individual clusters. This results in a data set of $\langle R_h(s) \rangle$ vs *s* that was well reproduced by the phenomenological relationship

$$\langle R_h(s) \rangle = 3.69 + 2.04 \times s - 0.069 \times s^2 \quad (10)$$

where $\langle R_h(s) \rangle$ is given in nm.

With this relationship and assuming hard sphere-like interactions between the different clusters, we can now calculate the concentration-dependence of both $\langle s \rangle_{w,app}$ and $\langle R_h(s) \rangle_{z,app}$. The expression for the measured apparent cluster size in this coarse-grained model is

$$\langle s \rangle_{w,app} = \langle s \rangle_w S^{eff}(0) \quad (11)$$

where $\langle s \rangle_w = \sum n(s)s^2 / \sum n(s)s$ is the true weight average cluster size, and $n(s)$ is the cluster size distribution obtained from the combination of Wertheim theory and HPT for a given concentration *C*. Note that the static structure factor S^{eff} introduced here has a different definition from $S(0)$ introduced in eq 8, and $S^{eff} = S(0)/\langle s \rangle_w$ now corresponds to the effective structure factor of a solution of hard spheres with a volume fraction ϕ_{HS}, reflecting the fact that the mAb clusters and not the individual antibodies are the new interacting objects. For hard spheres, we can exploit the Carnahan−Starling expression for the low wavevector limit of the static structure factor

$$S_{CS}(0) = \frac{(1 - \phi_{HS})^4}{(1 + 2\phi_{HS})^2 + \phi_{HS}^3(\phi_{HS} - 4)} \quad (12)$$

The only adjustable parameter introduced by this step is the conversion of the weight concentration into the effective hard sphere volume fraction ϕ_{HS} of the clusters.

The effective cluster HS volume fraction is calculated taking into account that the excluded volume contribution of an antibody in a cluster is equal to a sphere with a radius equal to the antibody radius of gyration R_g and that clusters are fractal, giving

$$\phi_{HS} = \left(\frac{2R_g}{\sigma_{HS}}\right)^3 \phi \langle s \rangle_n^{(3-d_F)/d_F} = 1.41 \phi \langle s \rangle_n^{(3-d_F)/d_F} \quad (13)$$

where $\sigma_{HS} = 2.9\sigma$ is the effective diameter of each antibody molecule (as determined in Figure 4), $d_F = 2.5$ is the fractal dimension of the clusters, ϕ is the nominal antibody volume fraction ($\phi = \pi/6\rho d^3$) based on the geometric diameter *d* of the molecule, and $\langle s \rangle_n = \sum n(s)s / \sum n(s)$ is the number average cluster size. Thus, in the coarse-grained model, we have an effective hard sphere volume fraction that is ∼40% higher than for the individual mAbs in the Wertheim analysis, which does not seem unrealistic, because clusters cannot overlap as much as individual antibodies do. The resulting comparison of the model calculations with experiments provides a very good description of the data, as shown in Figure 6a.

In order to calculate $\langle R_h \rangle_{z,app}$ we use the corresponding virial expression for the short-time collective diffusion coefficient, which results in

$$\langle R_h \rangle_{z,app} = \langle R_h(\langle s \rangle_z) \rangle / (1 + k_D \phi_{HS}) \quad (14)$$

where $k_D = 1.45$ for hard spheres.[45] Note that here we use the *z*-average aggregation number $\langle s \rangle_z = \sum n(s)s^3 / \sum n(s)s^2$ in order to calculate $\langle R_h(\langle s \rangle_z) \rangle$ from eq 10. The agreement for $\langle R_h \rangle_{z,app}$ with the results from the simple hard sphere model is quite good (Figure 6b), except for the highest values of *C*, where we

DOI: 10.1021/acs.molpharmaceut.9b00019
Mol. Pharmaceutics 2019, 16, 2394−2404

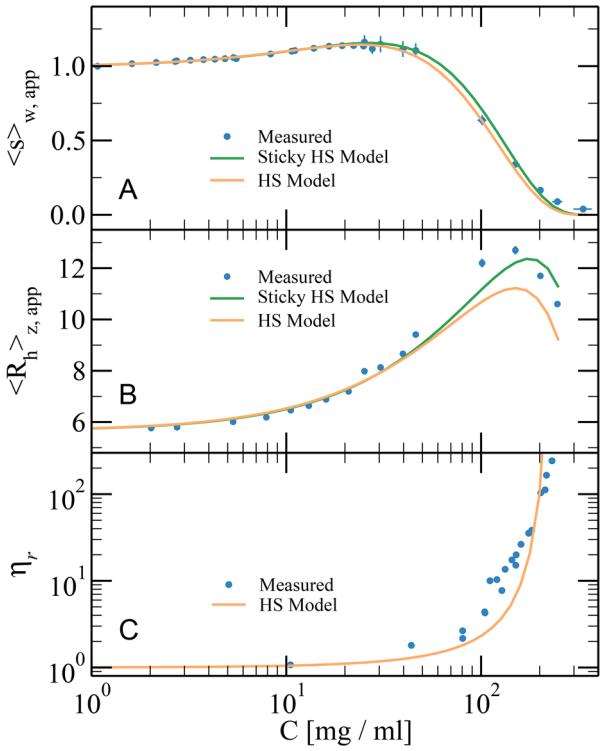

Figure 6. Comparison between experimental and theoretical results for the concentration-dependence of static and dynamic properties of the mAb solutions. Blue symbols are experimental data, while solid lines are the theoretical data for the hard sphere (orange line) and the sticky hard sphere (green line) models, respectively. The fit parameters are reported in Table S1. (a) Apparent aggregation number $\langle s \rangle_{w,app}$ vs weight concentration as determined by SLS; (b) apparent hydrodynamic radius $\langle R_h \rangle_{z,app}$ vs weight concentration from dynamic light scattering; (c) reduced viscosity η_r vs weight concentration measured by DLS-based microrheology.

expect eq 14 to fail; higher order terms should probably be included.

We also find that the apparent hydrodynamic radius obtained in DLS experiments is very sensitive to the interparticle interactions, and we can thus also look at a somewhat refined interaction model, where we include the possibility of an additional weak attraction between different clusters. When looking at the schematic description of the clusters in Figure 5, there will be unpaired patches for each cluster and, in particular, one negative *A* patch at the outside of each effective sphere, with which the unpaired *B* patches on mAbs located at the exterior of other clusters could interact. This can be included in our coarse-grained colloid model using the so-called adhesive or sticky hard sphere model,[46,47] where we include an additional weak short-range attractive potential between the clusters. In this model, eqs 12 and 14 then become

$$S_{SHS}(0) = \frac{(1-\phi_{HS})^4}{(1+2\phi_{HS}-\lambda\phi_{HS})^2} \tag{15}$$

and

$$\langle R_h \rangle_{z,app} = \langle R_h(\langle s \rangle_z) \rangle / (1 + (1.45 - 1.125/\tau)\phi_{HS}) \tag{16}$$

where τ is the stickiness parameter that is inversely proportional to the strength of the attractive interaction, and λ is given by

$$\lambda = 6(1-\tau+\tau/\phi_{HS})\left(1 - \sqrt{1 - \frac{1+2/\phi_{HS}}{6(1-\tau+\tau/\phi_{HS})^2}}\right) \tag{17}$$

The corresponding theoretical curves when τ is used as an additional fit parameter to the SLS and DLS data are also shown in Figure 6a,b. In particular, a better description of the apparent hydrodynamic radius is obtained within the SHS model with $\tau \approx 2.5$, corresponding to a very weak additional attraction between the mAb clusters. While the approximations made in our coarse-grained strategy may be too severe to say much about the exact nature of the effective interaction potential between the mAb clusters in solution, the experimental data are very well reproduced by our simple model. This indicates that the two chosen models, a pure hard sphere and an adhesive hard sphere interaction with moderate stickiness, likely bracket the true behavior of the self-assembling antibody investigated in this study.

Finally, as an ultimate test, we calculate the concentration-dependence of the relative viscosity η_r. We use the expression for η_r developed by Mooney, which is often and successfully applied for mono and polydisperse hard sphere colloidal suspensions[48]

$$\eta_r = e^{A\phi_{HS}/(1-\phi_{HS}/\phi_g)} \tag{18}$$

Here *A* is a constant, which for hard spheres is 2.5, and ϕ_g is the maximum packing fraction, which depends on the polydispersity of the system. In order to estimate it, we have evaluated the polydispersity of our antibody clusters as a function of concentration and find that at the highest studied concentration, it reaches about 45%. For such polydisperse hard spheres, the maximum packing fraction is ~0.71.[49] Using this value, we then should directly obtain the concentration-dependence of η_r from the previously determined relationship between *C* and ϕ_{HS} without any free parameter. The resulting comparison between the measured and calculated values of η_r is shown in the bottom panel of Figure 6, and the agreement is indeed quite remarkable given the lack of any free parameter. This clearly indicates that it is the excluded volume interactions between the self-associating clusters that are at the origin of the strong increase of the zero shear viscosity with increasing concentration, and our simple model is capable of predicting the measured *C*-dependence based on static and dynamic light scattering experiments quantitatively.

DISCUSSION

The self-assembly of monoclonal antibodies and its effect on the solution properties such as the viscosity are important factors in determining our ability to develop high concentration formulations. However, there has been a lack of decisive experimental and theoretical approaches to obtain a quantitative and predictive understanding of antibody solutions. A recent theoretical study has proposed a patchy model for antibody molecules,[50] in which different types of patch−patch attractions were considered, resulting in a large number of parameters to be adjusted to describe different experimental conditions. On the other hand, in the present work, we define the simplest possible model based on electrostatic calculations for the specific type of immunoglobulin, which we also study experimentally within the same buffer and salt conditions. This model is analytically solvable through the combination of Wertheim theory and hyper-

DOI: 10.1021/acs.molpharmaceut.9b00019
Mol. Pharmaceutics 2019, 16, 2394−2404

branched polymer theory, allowing us to predict the aggregation properties of the mAb solutions. We have shown that both thermodynamic properties and cluster distributions are in quantitative agreement with MC simulations of the model; thus, the theoretical predictions can be directly compared with experiments without suffering from numerical uncertainty. From the mAb self-assembly process built by the patchy interactions, we then employ a second coarse-graining step, in which we consider our antibody clusters as the elementary units. We thus use the most basic description considering these clusters interacting essentially as hard spheres or sticky hard spheres with very moderate attraction and apply available phenomenological descriptions to predict the dynamic properties of the system. This treatment essentially does not depend on any free parameter and is able to reproduce all measured data from SLS, DLS, and microrheology. This simple model, based on very fundamental assumptions, thus provides an elegant way to consistently describe the thermodynamic and dynamical behavior of mAb solutions.

The patchy model that we have established also provides a robust estimate of the attraction strength between patchy binding sites through Wertheim theory. To this aim, we have used the existing molecular information on the antibody structure to motivate the choice for the patchy site locations and the assumption of an attractive arm-to-tail interaction, while the strength of the interaction was determined from a fit of the experimental SLS data with the patchy model. However, we can make at least an attempt to compare the resulting attractive strength $\epsilon \approx 12.3 k_B T$ with the charge distributions given in Figure 1a. Summing up the partial charges, we obtain a total charge of +7 on the FAB domain and −1 on the FC domain. We can then model the two oppositely charged interaction sites as uniformly charged spheres of radius a and use a screened Coulomb potential of the form

$$U_{el}(r)/k_B T = Z_1 Z_2 \lambda_B \left(\frac{e^{\kappa a}}{1+\kappa a}\right)^2 \frac{e^{-\kappa r}}{r} \quad (19)$$

where $Z_1 = 7$ and $Z_2 = -1$ are the charges on the patches, $\lambda_B = e^2/4\pi\epsilon_0\epsilon k_B T = 0.7$ nm is the Bjerrum length, where e is the elementary charge, ϵ_0 is the vacuum permittivity, and ϵ is the relative dielectric constant, and $\kappa^{-1} = \sqrt{1/\left(4\pi\lambda_B \sum_j \rho_j z_j^2\right)} = 3$ nm is the Debye−Hückel screening length, with ρ_j being the number density of ions j with charge z_j. When using a patch size $a = \delta/2$ and a distance $r = \delta$ based on the model shown in Figure 1a, we obtain an interaction energy of $U_{el} = -12.7 k_B T$, which is remarkably close to the value obtained from the fit to the SLS data. It is clear that this calculation is only qualitative, and much more refined estimates of the actual interaction potential between identified interaction sites will be required. However, we believe that these results are indeed encouraging, and a more detailed experimental and numerical study, probing for example the ionic-strength-dependence of the self-association behavior of the mAb used here, will obviously be an important next step.

The qualitative agreement between our simple model and electrostatic calculations thus can be an ideal starting point to investigate and quantitatively assess the effects of additional excipients or chemical modifications on the antibody interaction. The model may therefore be used to estimate their effect on antibody stability and the resulting viscosity from molecular information. Such estimates are vital for an advanced formulation strategy where being able to discard unpromising candidates early is key. Moreover, the combination of static scattering data and Wertheim/HPT to determine the interaction strength and the cluster size distribution as a function of concentration and the subsequent test using DLS and (micro)rheology measurements without additional free parameters other than a rescaling of the volume fraction, allows us to critically test models for the type of interactions responsible for the self-association of a given mAb into clusters. It will be therefore interesting in the future to extend and test this type of approach to other proteins also displaying patchy interactions, given that they fulfill the assumption that each site can only bind to one other particle.

■ ASSOCIATED CONTENT

Supporting Information

The Supporting Information is available free of charge on the ACS Publications website at DOI: 10.1021/acs.molpharmaceut.9b00019.

Model fitting; generation of antibody clusters (PDF)

■ AUTHOR INFORMATION

Corresponding Authors

*E-mail: emanuela.zaccarelli@cnr.it. (E.Z.)
*E-mail: anna.stradner@fkem1.lu.se. (A.S.)

ORCID

Tommy Garting: 0000-0002-9423-1031
Peter Schurtenberger: 0000-0002-2790-8831
Emanuela Zaccarelli: 0000-0003-0032-8906
Anna Stradner: 0000-0003-3310-3412

Present Addresses

‖Copenhagen Business School, Porcelaenshaven 18B, 2000 Frederiksberg, Denmark (N.S.-G.)
⊥Computational Physics, University of Vienna, Sensengasse 8, 1090 Vienna, Austria (M.R.)

Author Contributions

C.R., P.S., E.Z., and A.S. designed research; N.S.-G., M.R., T.G., and E.Z. performed research; N.S.-G., M.R., T.G., C.R., P.S., E.Z., and A.S. discussed the science; N.S.-G., P.S., E.Z., and A.S. wrote the paper.

Notes

The authors declare no competing financial interest.

■ ACKNOWLEDGMENTS

This work was financed by the Swedish Research Council (VR; Grant No. 2016-03301), the Faculty of Science at Lund University, the Knut and Alice Wallenberg Foundation (project grant KAW 2014.0052), the European Research Council (ERC-339678-COMPASS and ERC-681597-MIMIC), and the European Union (MSCA-ITN COLLDENSE, grant agreement No. 642774).

■ REFERENCES

(1) Nelson, A. L.; Dhimolea, E.; Reichert, J. M. Development trends for human monoclonal antibody therapeutics. *Nat. Rev. Drug Discovery* **2010**, *9*, 767−774.
(2) Reichert, J. M. Marketed therapeutic antibodies compendium. *mAbs* **2012**, *4*, 413−415.

DOI: 10.1021/acs.molpharmaceut.9b00019
Mol. Pharmaceutics 2019, 16, 2394−2404

(3) Narasimhan, C.; Mach, H.; Shameem, M. High-dose monoclonal antibodies via the subcutaneous route: challenges and technical solutions, an industry perspective. *Ther. Delivery* **2012**, *3*, 889−900.
(4) Shire, S. J. Formulation and manufacturability of biologics. *Curr. Opin. Biotechnol.* **2009**, *20*, 708−714.
(5) Neergaard, M. S.; Kalonia, D. S.; Parshad, H.; Nielsen, A. D.; Mœ ller, E. H.; van de Weert, M. Viscosity of high concentration protein formulations of monoclonal antibodies of the IgG1 and IgG4 subclass - Prediction of viscosity through protein-protein interaction measurements. *Eur. J. Pharm. Sci.* **2013**, *49*, 400−410.
(6) Buck, P. M.; Chaudhri, A.; Kumar, S.; Singh, S. K. Highly Viscous Antibody Solutions Are a Consequence of Network Formation Caused by Domain-Domain Electrostatic Complementarities: Insights from Coarse-Grained Simulations. *Mol. Pharmaceutics* **2015**, *12*, 127−139.
(7) Godfrin, P. D.; Zarraga, I. E.; Zarzar, J.; Porcar, L.; Falus, P.; Wagner, N. J.; Liu, Y. Effect of Hierarchical Cluster Formation on the Viscosity of Concentrated Monoclonal Antibody Formulations Studied by Neutron Scattering. *J. Phys. Chem. B* **2016**, *120*, 278−291.
(8) Grimaldo, M.; Roosen-Runge, F.; Zhang, F.; Seydel, T.; Schreiber, F. Diffusion and Dynamics of γ-Globulin in Crowded Aqueous Solutions. *J. Phys. Chem. B* **2014**, *118*, 7203−7209.
(9) Yearley, E. J.; Godfrin, P. D.; Perevozchikova, T.; Zhang, H.; Falus, P.; Porcar, L.; Nagao, M.; Curtis, J. E.; Gawande, P.; Taing, R.; Zarraga, I. E.; Wagner, N. J.; Liu, Y. Observation of Small Cluster Formation in Concentrated Monoclonal Antibody Solutions and Its Implications to Solution Viscosity. *Biophys. J.* **2014**, *106*, 1763−1770.
(10) Bucciarelli, S.; Casal-Dujat, L.; De Michele, C.; Sciortino, F.; Dhont, J.; Bergenholtz, J.; Farago, B.; Schurtenberger, P.; Stradner, A. Unusual Dynamics of Concentration Fluctuations in Solutions of Weakly Attractive Globular Proteins. *J. Phys. Chem. Lett.* **2015**, *6*, 4470−4474.
(11) Foffi, G.; Savin, G.; Bucciarelli, S.; Dorsaz, N.; Thurston, G. M.; Stradner, A.; Schurtenberger, P. Hard sphere-like glass transition in eye lens Crystallin solutions. *Proc. Natl. Acad. Sci. U. S. A.* **2014**, *111*, 16748−16753.
(12) Cardinaux, F.; Zaccarelli, E.; Stradner, A.; Bucciarelli, S.; Farago, B.; Egelhaaf, S. U.; Sciortino, F.; Schurtenberger, P. Cluster-Driven Dynamical Arrest in Concentrated Lysozyme Solutions. *J. Phys. Chem. B* **2011**, *115*, 7227−7237.
(13) Lilyestrom, W. G.; Yadav, S.; Shire, S. J.; Scherer, T. M. Monoclonal Antibody Self-Association, Cluster Formation, and Rheology at High Concentrations. *J. Phys. Chem. B* **2013**, *117*, 6373−6384.
(14) Scherer, T. M.; Liu, J.; Shire, S. J.; Minton, A. P. Intermolecular Interactions of IgG1 Monoclonal Antibodies at High Concentrations Characterized by Light Scattering. *J. Phys. Chem. B* **2010**, *114*, 12948−12957.
(15) Yearley, E.; Zarraga, I.; Shire, S.; Scherer, T.; Gokarn, Y.; Wagner, N.; Liu, Y. Small-Angle Neutron Scattering Characterization of Monoclonal Antibody Conformations and Interactions at High Concentrations. *Biophys. J.* **2013**, *105*, 720−731.
(16) Scherer, T. M. Cosolute Effects on the Chemical Potential and Interactions of an IgG1 Monoclonal Antibody at High Concentrations. *J. Phys. Chem. B* **2013**, *117*, 2254−2266.
(17) Castellanos, M.; Pathak, J.; Leach, W.; Bishop, S.; Colby, R. Explaining the Non-Newtonian Character of Aggregating Monoclonal Antibody Solutions Using Small-Angle Neutron Scattering. *Biophys. J.* **2014**, *107*, 469−476.
(18) Corbett, D.; Hebditch, M.; Keeling, R.; Ke, P.; Ekizoglou, S.; Sarangapani, P.; Pathak, J.; Van Der Walle, C. F.; Uddin, S.; Baldock, C.; Avendaño, C.; Curtis, R. A. Coarse-Grained Modeling of Antibodies from Small-Angle Scattering Profiles. *J. Phys. Chem. B* **2017**, *121*, 8276−8290.
(19) Wertheim, M. S. Fluids with highly directional attractive forces. I. Statistical thermodynamics. *J. Stat. Phys.* **1984**, *35*, 19.
(20) Rubinstein, M.; Colby, R. H. *Polymer Physics*; Oxford University Press, 2003.
(21) Garting, T.; Stradner, A. Optical Microrheology of Protein Solutions Using Tailored Nanoparticles. *Small* **2018**, *14*, 1801548.
(22) Block, I. D.; Scheffold, F. Modulated 3D cross-correlation light scattering: Improving turbid sample characterization. *Rev. Sci. Instrum.* **2010**, *81*, 123107.
(23) Furst, E. M.; Squires, T. M. *Microrheology*; Oxford University Press, 2017.
(24) Roosen-Runge, F.; Zhang, F.; Schreiber, F.; Roth, R. Ion-activated attractive patches as a mechanism for controlled protein interactions. *Sci. Rep.* **2015**, *4*, 7016.
(25) Li, W.; Persson, B. A.; Morin, M.; Behrens, M. A.; Lund, M.; Zackrisson Oskolkova, M. Charge-induced patchy attractions between proteins. *J. Phys. Chem. B* **2015**, *119*, 503−508.
(26) McManus, J. J.; Charbonneau, P.; Zaccarelli, E.; Asherie, N. The physics of protein self-assembly. *Curr. Opin. Colloid Interface Sci.* **2016**, *22*, 73−79.
(27) Cai, J.; Sweeney, A. M. The Proof Is in the Pidan: Generalizing Proteins as Patchy Particles. *ACS Cent. Sci.* **2018**, *4*, 840−853.
(28) Ruzicka, B.; Zaccarelli, E.; Zulian, L.; Angelini, R.; Sztucki, M.; Moussaïd, A.; Narayanan, T.; Sciortino, F. Observation of empty liquids and equilibrium gels in a colloidal clay. *Nat. Mater.* **2011**, *10*, 56−60.
(29) Angelini, R.; Zaccarelli, E.; de Melo Marques, F. A.; Sztucki, M.; Fluerasu, A.; Ruocco, G.; Ruzicka, B. Glass−glass transition during aging of a colloidal clay. *Nat. Commun.* **2014**, *5*, 4049.
(30) Bomboi, F.; Romano, F.; Leo, M.; Fernandez-Castanon, J.; Cerbino, R.; Bellini, T.; Bordi, F.; Filetici, P.; Sciortino, F. Re-entrant DNA gels. *Nat. Commun.* **2016**, *7*, 13191.
(31) Sciortino, F.; Zaccarelli, E. Equilibrium gels of limited valence colloids. *Curr. Opin. Colloid Interface Sci.* **2017**, *30*, 90−96.
(32) Dolinsky, T. J.; Czodrowski, P.; Li, H.; Nielsen, J. E.; Jensen, J. H.; Klebe, G.; Baker, N. A. PDB2PQR: expanding and upgrading automated preparation of biomolecular structures for molecular simulations. *Nucleic Acids Res.* **2007**, *35*, W522.
(33) Jurrus, E.; et al. Improvements to the APBS biomolecular solvation software suite. *Protein Sci.* **2018**, *27*, 112−128.
(34) Bianchi, E.; Largo, J.; Tartaglia, P.; Zaccarelli, E.; Sciortino, F. Phase diagram of patchy colloids: Towards empty liquids. *Phys. Rev. Lett.* **2006**, *97*, 168301.
(35) Tavares, J. M.; Teixeira, P. I. C.; Telo da Gama, M. M.; Sciortino, F. Equilibrium self-assembly of colloids with distinct interaction sites: Thermodynamics, percolation, and cluster distribution functions. *J. Chem. Phys.* **2010**, *132*, 234502.
(36) Hansen, J.-P.; McDonald, I. R. *Theory of simple liquids*, 3rd ed.; 2006.
(37) Jackson, G.; Chapman, W. G.; Gubbins, K. E. Phase equilibria of associating fluids: Spherical molecules with multiple bonding sites. *Mol. Phys.* **1988**, *65*, 1−31.
(38) Bianchi, E.; Tartaglia, P.; Zaccarelli, E.; Sciortino, F. Theoretical and numerical study of the phase diagram of patchy colloids: Ordered and disordered patch arrangements. *J. Chem. Phys.* **2008**, *128*, 144504.
(39) Tavares, J. M.; Teixeira, P. I. C.; Telo da Gama, M. M. How patchy can one get and still condense? The role of dissimilar patches in the interactions of colloidal particles. *Mol. Phys.* **2009**, *107*, 453−466.
(40) Schurtenberger, P.; Cavaco, C.; Tiberg, F.; Regev, O. Enormous Concentration-Induced Growth of Polymer-like Micelles. *Langmuir* **1996**, *12*, 2894−2899.
(41) Schurtenberger, P.; Scartazzini, R.; Luisi, P. L. Viscoelastic properties of polymerlike reverse micelles. *Rheol. Acta* **1989**, *28*, 372−381.
(42) Murphy, R.; Slayter, H.; Schurtenberger, P.; Chamberlin, R.; Colton, C.; Yarmush, M. Size and Structure of Antigen-Antibody Complexes - Electron Microscopy and Light Scattering Studies. *Biophys. J.* **1988**, *54*, 45−56.
(43) Schurtenberger, P.; Newman, M. E. *Environmental Particles*; Lewis Publishers, 1993; Vol. 2; pp 37−115.

DOI: 10.1021/acs.molpharmaceut.9b00019
Mol. Pharmaceutics 2019, 16, 2394−2404

(44) Ortega, A.; Amorós, D.; García de la Torre, J. Prediction of Hydrodynamic and Other Solution Properties of Rigid Proteins from Atomic- and Residue-Level Models. *Biophys. J.* **2011**, *101*, 892−898.
(45) Banchio, A. J.; Nagele, G. Short-time transport properties in dense suspensions: From neutral to charge-stabilized colloidal spheres. *J. Chem. Phys.* **2008**, *128*, 104903.
(46) Piazza, R.; Peyre, V.; Degiorgio, V. Sticky hard spheres model of proteins near crystallization: A test based on the osmotic compressibility of lysozyme solutions. *Phys. Rev. E: Stat. Phys., Plasmas, Fluids, Relat. Interdiscip. Top.* **1998**, *58*, R2733−R2736.
(47) Cichocki, B.; Felderhof, B. U. Diffusion coefficients and effective viscosity of suspensions of sticky hard spheres with hydrodynamic interactions. *J. Chem. Phys.* **1990**, *93*, 4427−4432.
(48) Mooney, M. The viscosity of a concentrated suspension of spherical particles. *J. Colloid Sci.* **1951**, *6*, 162.
(49) Farr, R. S.; Groot, R. D. Close packing density of polydisperse hard spheres. *J. Chem. Phys.* **2009**, *131*, 244104.
(50) Kastelic, M.; Dill, K. A.; Kalyuzhnyi, Y. V.; Vlachy, V. Controlling the viscosities of antibody solutions through control of their binding sites. *J. Mol. Liq.* **2018**, *270*, 234.

DOI: 10.1021/acs.molpharmaceut.9b00019
Mol. Pharmaceutics 2019, 16, 2394−2404